First-Epoch VSOP Observation of 3C 380: Kinematics of the Parsec-Scale Jet

Seiji Kameno, Makoto Inoue, and Kenta Fujisawa National Astronomical Observatory, 2-21-1 Osawa, Mitaka, Tokyo 181-8588 E-mail (SK) kameno@hotaka.mtk.nao.ac.jp

and

Zhi-Qiang Shen and Kiyoaki Wajima The Institute of Space and Astronautical Science, 3-1-1 Yoshinodai, Saqamihara, Kanaqawa 229-8510

(Received 2000 July 7; accepted 2000 October 18)

Abstract

The space-VLBI mission VSOP provides high-quality imaging capabilities to investigate fine structures in quasar jets. We report on the first-epoch VSOP observation of the superluminal quasar 3C 380 at $\lambda 6$ cm. A high-quality image with a dynamic range of 1:1200 at a resolution of 0.74 mas \times 0.36 mas reveals precise structure along the pc-scale jet. Components C2, A, and F, have been identified with those in previous ground-VLBI observations, and an apparent superluminal motion has been confirmed. We find a very straight motion with a constant apparent velocity for components A and F. Each motion vector is almost parallel to each position vector. This suggests a ballistic ejection from the core. In spite of better position accuracy than previous ground-VLBI observations, we cannot confirm any evidence of acceleration or changes of the position angle which were reported in Polatidis and Wilkinson (1998, AAA 069.159.023). We confirmed that the bent jet structure has kept its similarity and direction, compared with previous images. This suggests an oblique shock in relativistic flow rather than the Kelvin–Helmholtz instability.

Key words: galaxies: active — galaxies: jets — quasars: individual (3C 380 = 1828+487) — radio continuum: galaxies — techniques: interferometric

1. Introduction

A relativistic jet associated with active galactic nuclei (AGNs) is one of the most spectacular phenomena in the universe. They stimulate fundamental questions: how can a jet become accelerated to a speed approaching the speed of light, and does the apparent motion of knots in AGN jets imply bulk motion or shock propagation? To clarify the nature of relativistic jets, a kinematic analysis based on high-quality images with a sufficient resolution is important.

The quasar 3C 380 (1828+487) is one of the most powerful radio sources at a redshift of z=0.692. If we assume the Hubble constant of $H_0=75~\rm km~s^{-1}~Mpc^{-1}$, 1 mas (milli-arcsec) corresponds to 6 pc. This object is classified as a compact steep-spectrum (CSS) source, with an overall size of 10 kpc and a steep spectrum of $\alpha=d\log S_{\nu}/d\log \nu=-0.7$ (Fanti et al. 1990). Wilkinson et al. (1984) revealed a kpc-scale structure consisting of a jet in P.A.= 308°, a complex of knots at 1" at the end of the jet, and an arc with an extent of ~ 8 ". The complex of knots includes a hot spot at 0."73 from the core, which can be seen at optical wavelength,

showing a synchrotron spectrum with $\alpha = -0.97$ (O'Dea et al. 1999). Wilkinson et al. (1991) found a superluminal motion of $\mu = 0.36 \pm 0.09$ mas yr⁻¹ or $\beta_{app} = 10.5 \pm 2.7$ in 100-pc-scale jet. They also detected the depolarization anisotropy, indicating a larger Faraday depth towards the counter-jet side, and then concluded that this object is a Fanaroff-Riley class II source (Fanaroff, Riley 1974) seen approximately end-on. Kameno et al. (1995) measured a millimeter-wave spectrum and derived a spectral index between 22 and 92 GHz of $\alpha_{22}^{92} = -0.53$. Detailed jet structures and kinematics in pc-scale have been studied by extensive multi-epoch VLBI observations (Polatidis, Wilkinson 1998; hereafter PW98). The jet shows a bent structure in 100-pc scale. Several knots have been identified along the jet. PW98 has monitored a motion of the knot component A, which locates at ~ 50 pc from the core, and measured an apparent superluminal motion of $\beta_{\rm app} = 5.9 \pm 0.7$. It was found that component A curved along the bending jet, and that its apparent speed changed by $\beta_{app} = 2$ to 10; they thus mentioned the intersection of oblique shocks. This idea suggests astrophysical interest: 3C 380 can be a good probe to investigate an interaction between a relativistic jet and the ambient gas. Taylor (1998) performed a VLBI polarimetry and displayed magnetic fields along the jet. He found that the core is weakly polarized, and that the polarization degree increases downstream and reaches a maximum of 13% at component A. The core component shows a convex spectrum peaked at ~ 10 GHz, which implies synchrotron self-absorption at a frequency below the peak (Kameno et al. 1995).

This object stimulates interests related to the kinematics and geometry of relativistic jets. First, several distinct knots allow us to measure their apparent motions by multi-epoch observations with less chance to misidentify. Component A, for instance, has been clearly identified since 1982, as reviewed above. Second, the small viewing angle of the jet magnifies any small changes of the jet motion. This effect allows us to accurately investigate the kinematics of a jet, such as acceleration, deceleration, or curving motions, if any. Third, the bending structure of the jet could be a key for understanding the properties of the jet. It may demonstrate the Kelvin-Helmholtz instability as being the result of an interaction between the relativistic flow and external materials, as stated by PW98. To clarify these processes, the space-VLBI system is the best device to provide a sufficient image quality and resolution. In this paper, we present the first-epoch VSOP (Hirabayashi et al. 1998) observation at λ 6 cm concentrated on the kinematics of a pc-scale jet. We have also observed 3C 380 at λ 18 cm to investigate the distribution of the spectral index, which will be reported elsewhere.

2. Observations

2000PASJ...52.1045K

Our VSOP observation at $\lambda 6$ cm (4816 MHz) was carried out on 1998 July 4. We used two baseband converters with a 16-MHz bandwidth. The synthesized VLBI array consisted of a spacecraft and eleven ground radio telescopes. The spacecraft HALCA (Hirosawa et al. 1998) was tracked by the Madrid (Spain) and Goldstone (USA) tracking stations for the purpose of providing an uplink phase transfer and downlink data transmission. Baselines with HALCA contribute to visibilities at a high spatial frequency range of $120 < \sqrt{u^2 + v^2} < 460 \text{ M}\lambda$. The ground array consists of ten VLBA stations in the USA and the Effelsberg 100-m radio telescope in Germany. The correlation process was accomplished by the NRAO VLBA correlator in Socorro, NM, USA. We used the Astronomical Image Processing System (AIPS) developed by the NRAO for fringe fitting, passband calibration, and a priori amplitude calibration processes. Fringes were detected in all valid visibilities with signal-to-noise ratios > 10 for 3-min coherent integration. The distribution of the visibilities in the spatial frequency domain (uv coverage) is shown in figure 1. Figure 2 shows the visibility

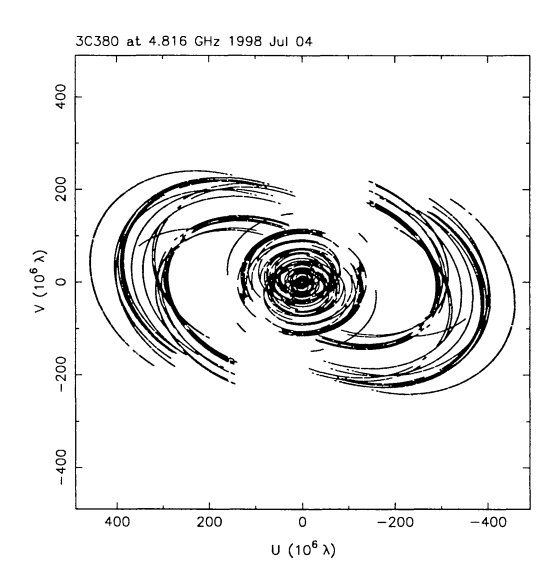


Fig. 1. Distribution of the visibilities in the spatial frequency plane (uv coverage). The inner circular concentration consists of ground-only baselines, while the spacecraft HALCA contributes to outer extension

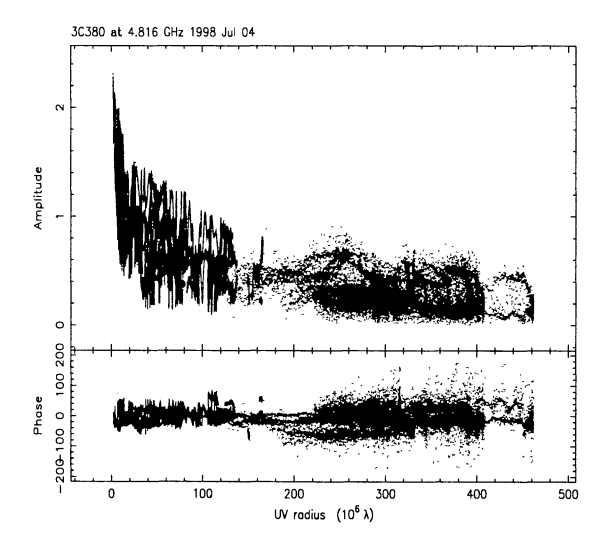


Fig. 2. Visibility amplitudes (top) in Jy and phases (bottom) in degree as a function of the uv distance (= $\sqrt{u^2 + v^2}$). HALCA contributes to visibilities at > 120 M λ .

amplitudes and phases as a function of the uv distance $(\sqrt{u^2 + v^2})$.

We produced synthesized images using Difmap (Shepherd 1997). Since 3C 380 has extended structures at the arcsec scale (O'Dea et al. 1999), we took four steps with different subsets of radio telescopes before producing the final image. We started from the most compact array, which consists of five VLBA telescopes (PT, LA, FD, KP, and OV). In this step, we confirmed a knot

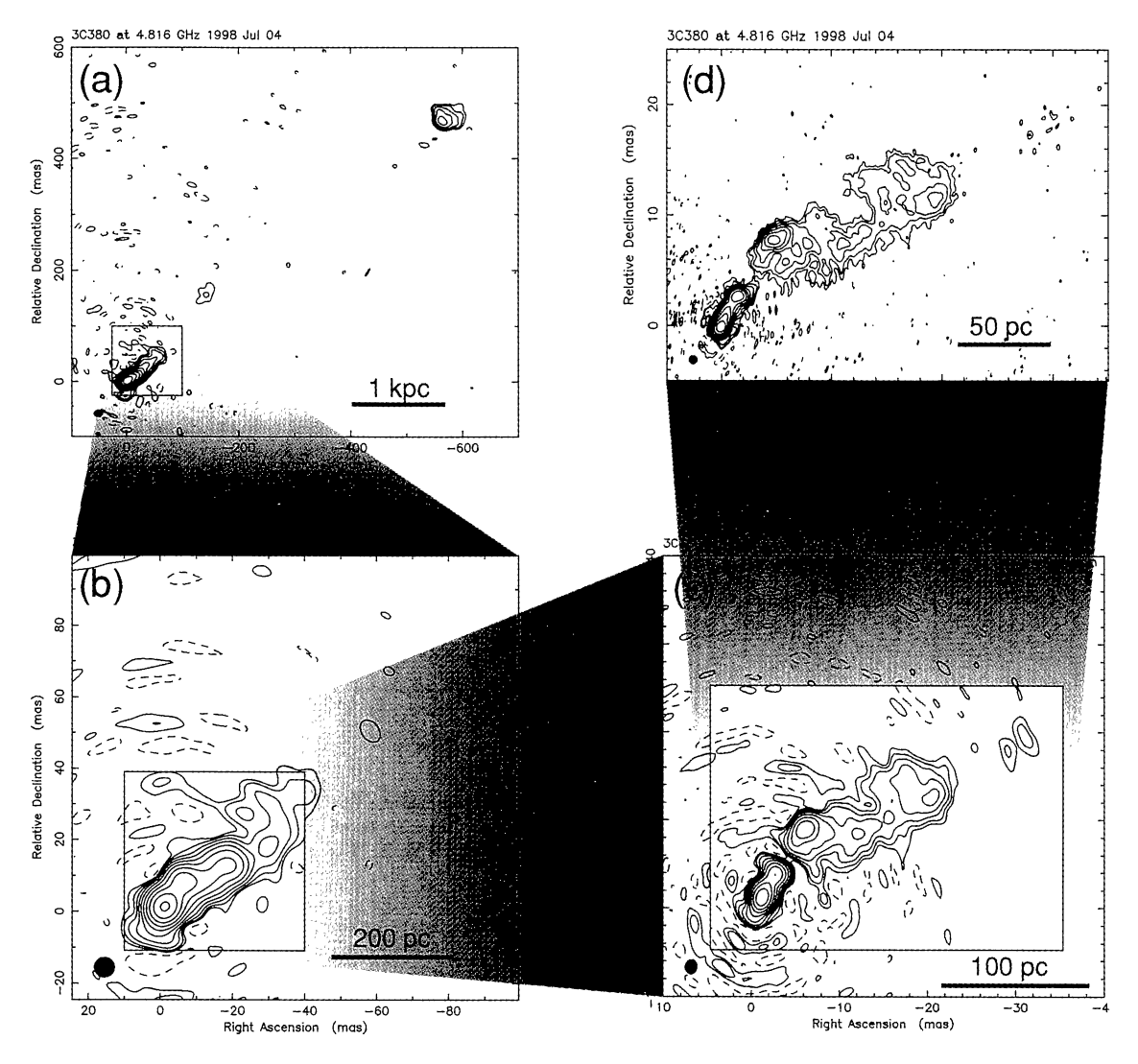


Fig. 3. (a) Image with a resolution of 15 mas × 12 mas in P.A. = -83°8 obtained by the most compact array consisting of five VLBA telescopes (PT, LA, FD, KP, and OV). Contour levels are 1.314 × (-1,1,2,4,..., and 512) mJy beam⁻¹. (b) Image with a resolution of 5.6 mas × 5.47 mas in P.A. = 81°3 by an array of eight VLBA telescopes (PT, LA, FD, OV, KP, NL, HN, and BR). The contour levels are 1.617 × (-1,1,2,4,..., and 512) mJy beam⁻¹. (c) Image with a resolution of 1.65 mas × 1.37 mas in P.A. = -7°67 by the full ground array of eleven telescopes (ten VLBA telescopes and Effelsberg). The contour levels are 1.389 × (-1,1,2,4,..., and 256) mJy beam⁻¹. (d) Image of the full synthesized array including the spacecraft HALCA, restored with a circular 0.75 mas beam. The contour levels are 0.969 × (-1,1,2,4,..., and 256) mJy beam⁻¹. Each lowest contour is 3σ level. See also table 1 for array configurations and image performances.

component at 750 mas from the brightest peak. Since the knot contributes to tiny ripples in the visibilities, this step was important to obtain a high dynamic range in the final image. In the second step, we added three VLBA telescopes (BR, NL, and HN) to image diffuse emission on the 100-pc scale. All 11 ground telescopes contributed to the third step. Finally, we added spaceground baselines to obtain a high-resolution image. The fourth image was taken by restoring a circular 0.75 mas beam. By taking uniform weighting with scaling by errors raised to the power -0.5, we obtained a synthesized

beam FWHM of $0.74 \text{ mas} \times 0.36 \text{ mas}$ at P.A. = $-7.^{\circ}8$. At every step, phase-only self-calibration processes were applied before we made an amplitude self-calibration at once.

3. Results

3.1. Image Performance

In the four steps, we obtained four images with different resolutions. These images are shown in figure 3 to demonstrate the relation between kpc- and pc-scale

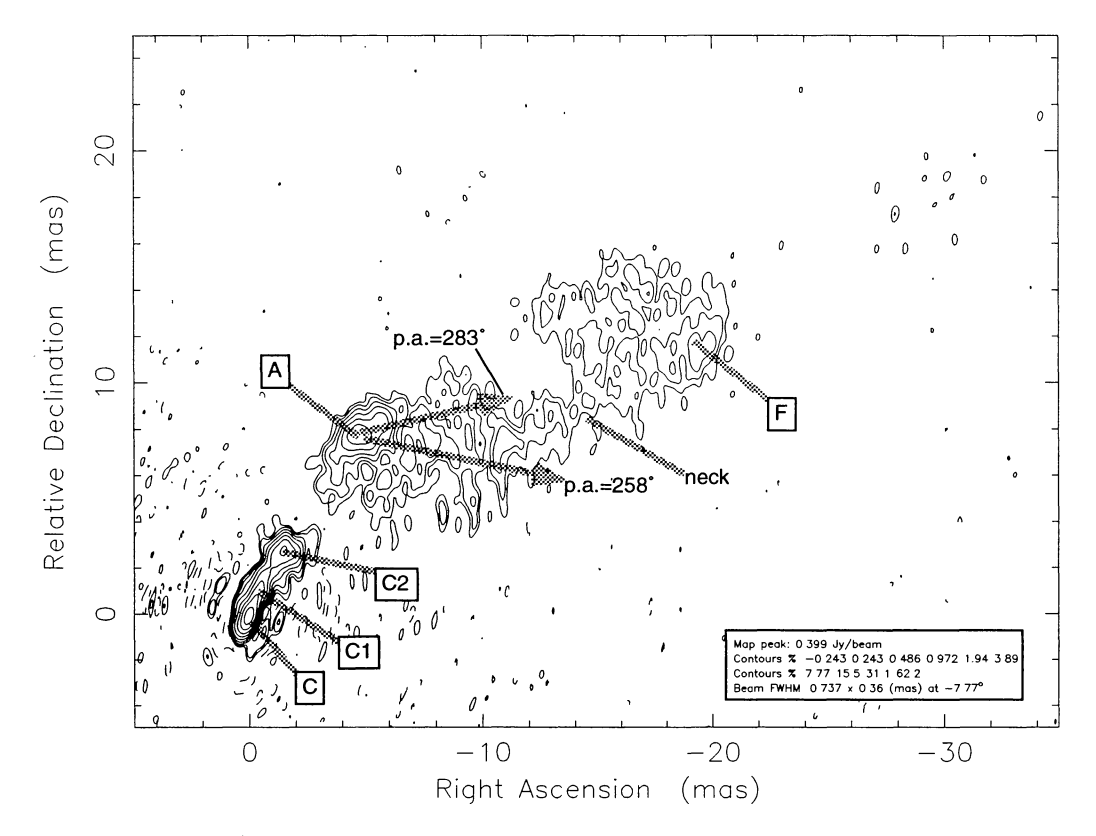


Fig. 4. The λ 6 cm (4816 MHz) VSOP image of 3C 380 with a synthesized beam of 0.74 mas \times 0.36 mas in P.A. = -7° 8. The r.m.s. noise level is $\sigma = 0.323$ mJy beam⁻¹. The contours start at $\pm 3\sigma$ level, as well as figure 3, increasing by a factor of 2. Components C, C1, C2, A, and F are identified as those in PW98. The arrows from component A indicate the direction of the ridge lines reported by PW98.

Figure 4 shows the final image. It atstructures. tributes to a high dynamic range of 1:1200 (ratio between r.m.s. noise level and peak brightness), which allows us to identify the components in the jet. We also attempted equal weighting to enhance the resolution (FWHM 0.64 mas \times 0.30 mas at P.A. = $-7.^{\circ}$ 8), as shown in figure 5. The performance of these images are listed in table 1. The r.m.s. noise of each image is derived from the residual visibilities after subtracting those calculated from CLEAN components. The r.m.s. was approximately twice (agreement factor of 1.8) as large as that of a statistical estimation based on the errors and the weights of the visibilities. This means that the set of CLEAN components does not completely represent what the brightness distribution really is; nevertheless, the agreement factor of 1.8 is fairly good for VLBI imaging.

3.2. Identification of Components

In figure 3a with the lowest resolution, the knot at 750 mas from the brightest peak is identified with "knot 1" detected with the VLA and the Hubble space telescope by O'Dea et al. (1999). We identify components C, C1, C2, A, and F, which were labeled by PW98.

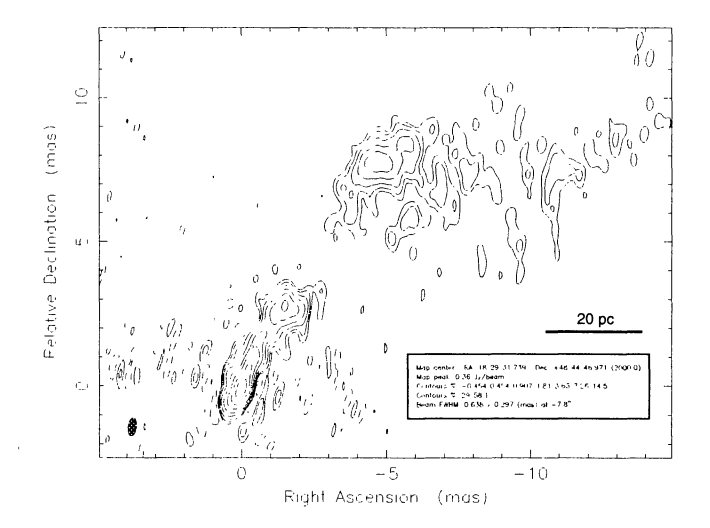


Fig. 5. $\lambda 6$ cm VSOP image focusing on the core and pc-scale jets. Equal weights regardless of the errors enhance the resolution (FWHM of 0.64 mas \times 0.30 mas in P.A. = $-7.^{\circ}8$), but lose some dynamic range. The contour levels are $1.631 \times (-1, 1, 2, 4, \ldots)$, and 128) mJy beam⁻¹.

${\bf Antennae^*}$	Synthesized beam			Peak intensity	r.m.s. noise	
	Major axis Minor axis (mas) (mas)		P.A. (°)	(Jy beam ⁻¹)	(mJy beam ⁻¹)	
(a) PT, LA, FD, OV, KP	15	12	-83.8	1.19	0.44	
(b) PT, LA, FD, OV, KP, NL, HN, BR	5.6	5.47	81.3	0.923	0.54	
(c) PT, LA, FD, OV, KP, NL, HN, BR, SC, MK, EB	1.65	1.37	-7.67	0.664	0.46	
$(d)^{\dagger}$ PT, LA, FD, OV, KP, NL, HN, BR, SC, MK, EB, HALCA	0.75	0.75	•••	0.467	0.323	
PT, LA, FD, OV, KP, NL, HN, BR, SC, MK, EB, HALCA	0.74	0.36	-7.77	0.399	0.323	
PT, LA, FD, OV, KP, NL, HN, BR, SC, MK, EB, HALCA [‡]	0.64	0.30	-7.80	0.360	0.543	

^{*}PT: Pie Town NM USA, LA: Los Alamos NM USA, FD: Fort Davis TX USA, OV: Owens Valley CA USA, KP: Kitt Peak AZ USA, NL North Liberty IA USA, HN: Hancock NH USA, BR: Brewster WA USA, SC: Saint Croix VI USA, MK: Mauna Kea HI USA, EB: Effelsberg Germany, HALCA: spacecraft in orbit.

Table 2. Parameters of the Gaussian components by IMFIT in AIPS.

Component	Flux density	Relative position*		
	(mJy)	Distance (mas)	P.A. (°)	
C	659.5 ± 1.3	• • •		
C1	458.2 ± 1.5	0.46 ± 0.05	352.5 ± 6.4	
$C2 \dots$	229.6 ± 1.2	3.15 ± 0.05	332.5 ± 0.9	
A	240.3 ± 1.5	9.22 ± 0.05	328.8 ± 0.3	
$\mathbf{F}\dots$	134.5 ± 1.0	22.17 ± 0.25	302.0 ± 0.6	

^{*}Position errors are set to one-tenth of the beam size.

Components B, D, and E in PW98 seem to be amorphous in our high-resolution image. In our image, we confirm that the jet bends at A, as reported by PW98. While the ridge is fuzzy in ~ 7 mas from component A, it converges within a narrow neck at 10 mas from A (see figure 4). The average direction from A to the neck points to P.A. = 277° .

We measured the positions of these components relative to the core component C, by applying a Gaussian fit using the task 'IMFIT' in the AIPS. The results are listed in table 2. After we measured the positions of the identified components relative to the core, we compared them with those measured by PW98. Observations by Taylor (1998) at 15 GHz in 1997.07 also helped in the identifi-

cation; however, we did not include their results in later calculations of the proper motion because of a different frequency and a lack of errors in their position measurements.

Since components F and A are clearly separated from others, we estimated the apparent velocity by using all measurements by PW98 and our results. The distance of A from the core is 9.22 ± 0.05 mas in 1998.5, as expected from an extrapolation using PW98 and Taylor (1998). Component F appears at 22.17 ± 0.25 mas from the core, where it is also expected to be.

Although component C2 is clearly distinguishable from other components in our image, the identification of components C, C1, and C2 includes ambiguities. Though PW98 distinguished C1 from C2 at $\lambda 1.3$ cm, they labeled C12 as a merger of C1 and C2 at $\lambda 6$ cm. Insufficient resolutions at $\lambda 6$ cm in PW98 could result in a smeared position accuracy for C2. Therefore, we estimated the apparent velocity of C2 by comparing the positions at $\lambda 1.3$ cm by PW98 and our results at $\lambda 6$ cm. Its distance of 3.0 mas at 15 GHz in 1997.07 (Taylor 1998) is located close to our result at 3.15 ± 0.05 mas.

For the same reason, we used the positions at $\lambda 1.3$ cm by PW98 and ours at $\lambda 6$ cm, to calculate the apparent velocity of C1. While PW98 and we measured the separation of 0.23 mas in 1990.8 and 0.46 ± 0.05 mas in 1998.5, respectively, Taylor (1998) reported 1.0 mas in 1997.07 (see figure 6). This discrepancy indicates that the identification of C1 is not reliable, probably due to differences

[†]Restored image with a circular Gaussian beam.

[‡]Equal weight regardless of errors of visibilities.

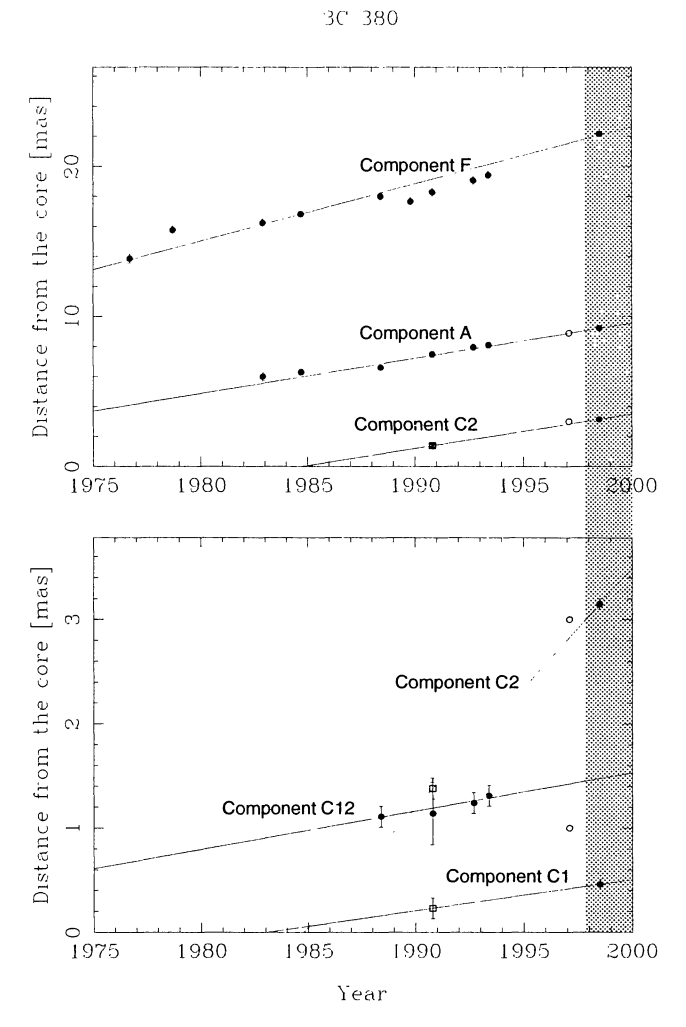


Fig. 6. Distance of components from the core as a function of observed epoch. The measurements in 1998.5 (grey area) are our results. See table 2 for the numerical value. The data before 1993.4 are from the literature given in PW98. The open squares indicate 22-GHz observations. Measurements in 1997.1 at 15 GHz (open circles) by Taylor (1998) are also plotted, though they are not used for calculations of the apparent velocities, because the errors are not stated. The solid lines show a weighted least-squares linear fit, whose results are given in table 3.

in the frequencies and the optically-thick spectrum of C1. Table 3 and figure 6 show the results of a weighted least-squares linear fit for the apparent velocity of the components. Even though the fit for component C1 appears in table 4, we are not confident about it, as mentioned above. The result of C12 is also included for the purpose of a comparison.

4. Discussion

4.1. The Core

Component C, which is considered to be the core, is resolved in the image with equal visibility weights (figure 5). The visibilities with HALCA allowed us to measure the FWHM size (ϕ) of C for the first time, which result in $\phi_{\rm maj}=0.70\pm0.01$ mas in P.A. = 340° and $\phi_{\rm min}=0.21\pm0.01$ mas. The major axis close to the jet axis implies that component C is a complex of the nucleus and newly ejected knots. Using the size and flux density (S) of 659.5 \pm 1.3 mJy, we calculated the brightness temperature of the Gaussian model using

$$T_{\rm b} = 1.224 \times 10^{12} \left(\frac{S}{1 \,\text{Jy}}\right) \left(\frac{\phi_{\rm maj}}{1 \,\text{mas}}\right)^{-1} \times \left(\frac{\phi_{\rm min}}{1 \,\text{mas}}\right)^{-1} \left(\frac{\nu}{1 \,\text{GHz}}\right)^{-2} \text{K}. \tag{1}$$

This gave $T_{\rm b}=(2.4\pm0.1)\times10^{11}~{\rm K}$ in the observer's frame, or $(4.1\pm0.2)\times10^{11}~{\rm K}$ in the rest frame. The Doppler factor (δ) of the core can be estimated using the size and the peak frequency, if we assume energy equipartition between the particles and the magnetic field (Scott, Readhead 1977; Readhead 1994), by the following equation:

$$\delta = \left[\left(\frac{10^3 F(\alpha)}{1.8 \phi} \right)^{34} \left(\frac{2h}{1 - \frac{1}{\sqrt{1+z}}} \right)^2 (1+z)^{15-2\alpha} \right.$$

$$\times S_{\rm m}^{16} \left(10^3 \nu_{\rm m} \right)^{-35-2\alpha} \right]^{\frac{1}{13-2\alpha}}. \tag{2}$$

Here, $S_{\rm m}$ is the peak flux density in Jy at the peak frequency $(\nu_{\rm m})$ in GHz, and h is a parameter related to the Hubble constant, $H_0=100h~{\rm km~s^{-1}~Mpc^{-1}}$. We take h=0.75. $F(\alpha)$ is a numerical function given by Scott and Readhead (1977). We multiply ϕ by 1.8 to adjust for a spherical source (Marscher 1987). Millimeter-wave observations by Kameno et al. (1995) give $\alpha=-0.53$, $S_{\rm m}=1.8\pm0.3$ Jy, and $\nu_{\rm m}=9.7\pm0.9$ GHz. $F(\alpha)=3.6$ for $\alpha=-0.53$. Then, we have $\delta=1.12\pm0.36$.

In many superluminal radio sources, the observed flux densities ($S_{\rm ob}$) of AGN jets are amplified by a Doppler-boosting effect, as expressed by the following formula (Blandford et al. 1977).

$$S_{\rm ob}(\nu) = S(\nu)\delta^{2-\alpha}.\tag{3}$$

In the case of 3C 380 core, however, $\delta \simeq 1$ does not cause any amplification of the brightness. The bulk Lorentz factor (γ) can be estimated by the relation

$$\gamma = \frac{\beta_{\text{app}} + \delta^2 + 1}{2\delta}.\tag{4}$$

Epoch W	Wavelength	Wavelength Component F		Component A		Component C2		Ref.
	(cm)	Distance (mas)	P.A. (°)	Distance (mas)	P.A. (°)	Distance (mas)	P.A. (°)	
1976.7	6	13.86 ± 0.30	302.48	•••				1
1978.7	6	15.76 ± 0.25	304.68					1
1982.9	6	16.23 ± 0.25	304.57	5.99 ± 0.28	329.06			1
1984.7	6	16.82 ± 0.18	303.29	6.29 ± 0.20	329.00			1
1988.4	6	17.99 ± 0.25	306.37	6.60 ± 0.10	331.51			1
1989.8	6	17.64 ± 0.25	305.40				• • •	1
1990.8	6	18.26 ± 0.25	304.55	7.48 ± 0.21	330.07			1
1990.8	1.3					1.38 ± 0.02	334.6	1
1992.7	6	19.06 ± 0.25	303.29	7.95 ± 0.22	329.99			1
1993.4	6	19.42 ± 0.25	302.67	8.10 ± 0.20	329.56			1
1997.1	2			8.9	327.34	3.00	332.5	2
1998.5	6	22.17 ± 0.05	302.0	9.22 ± 0.05	302.00	3.15 ± 0.05	332.5	3

References: (1) Polatidis, Wilkinson 1998; (2) Taylor 1998; (3) this paper.

Table 4. Position change of components C1 and C12*.

Epoch	Wavelength	Component C1		Component C12		Ref.
	(cm)	Distance (mas)	P.A. (°)	Distance (mas)	P.A. (°)	
1988.4	6	• • •		1.11 ± 0.1	331.5	1
1990.8	6			1.14 ± 0.3	334.1	1
1990.8	1.3	0.23 ± 0.02	326.3			1
1992.7	6			1.24 ± 0.1	335.5	1
1993.4	6			1.31 ± 0.1	334.3	1
1997.1	2	1.0	326.3			2
1998.5	6	0.46 ± 0.05	352.5			3

^{*}Component C12 is a complex of C1 and C2 when resolution is insufficient to isolate them.

References: (1) Polatidis, Wilkinson 1998 (2) Taylor 1998 (3) this paper.

We then have $\gamma=1.01^{+0.07}_{-0.01}$, under the condition of $\beta_{\rm app}\ll 1$. This brief result indicates that the core is non-relativistic. Otherwise, it would be far from the equipartition condition.

4.2. The Parsec-Scale Jet

Component A shows an apparent proper motion of $\mu=0.235\pm0.006$ mas yr⁻¹, corresponding to an apparent velocity of $\beta_{\rm app}=6.86\pm0.18$ in the time range 1982.9 to 1998.5. This average proper motion is consistent with that in the time range 1982.9 to 1993.4 by PW98. Although PW98 reported that A apparently accelerated to $\beta_{\rm app}=10.3\pm2.7$ between 1990.8 and 1993.4, the latest average proper motion between 1990.8 and 1998.5 of $\mu=0.223\pm0.006$ mas yr⁻¹ ($\beta_{\rm app}=6.51\pm0.17$) implies a constant apparent velocity. Because the position angle of A showed no significant change during the period, the

reported curving motion is not likely to be real. We cannot confirm any evidence for the apparent acceleration of component A.

The position angle of the proper motion vector between 1982.9 and 1998.5 is $324^{\circ} \pm 1.^{\circ}9$, which is almost parallel to the position vector of A at P.A. = $328.^{\circ}8 \pm 0.^{\circ}3$ with respect to the core. This suggests that A is ballistically ejected from the core.

As reviewed by Blandford et al. (1977), or Pearson and Zensus (1987), an apparent superluminal motion requires extremely relativistic velocity. The minimum intrinsic velocity β_{\min} , the minimum Lorentz factor γ_{\min} , and the maximum viewing angle θ_{\max} can be obtained by

$$\beta_{\min} = \frac{\beta_{\text{app}}}{\sqrt{1 + \beta_{\text{app}}^2}},\tag{5}$$

$$\gamma_{\min} = \sqrt{1 + \beta_{\rm app}^2},\tag{6}$$

$$\theta_{\text{max}} = 2 \arctan \frac{1}{\beta_{\text{app}}}.$$
 (7)

For component A, we have $\beta_{\min} = 0.9895$, $\gamma_{\min} = 6.86$, and $\theta_{\max} = 16.^{\circ}6$.

Component F shows an extended feature which is extremely resolved in our image. To avoid difficulties in identifying the reference position, we used a circular 2.5mas restoring beam before applying IMFIT to measure its position. The average proper motion of F between 1976.7 and 1998.5 is $\mu = 0.381 \pm 0.005$ mas yr⁻¹, or $\beta_{\rm app} = 11.1 \pm 0.15$. This is significantly larger than the measurements by PW98 $\mu = 0.276 \pm 0.015$ mas yr⁻¹ between 1976.7 and 1993.4; nevertheless, as pointed out by PW98, the formal errors seem to be too small without uncertainties due to the extended structure. The proper motion vector of F points to P.A. = $295.^{\circ}4 \pm 0.^{\circ}8$, which is approximately parallel to the position vector at P.A. = $302.^{\circ}0 \pm 0.^{\circ}1$. This also suggests a ballistic ejection of component F, the same as that of component A. We derived kinematic parameters of F, $\beta_{\min} = 0.9960$, $\gamma_{\min} = 11.2$, and $\theta_{\max} = 10.^{\circ}3$.

Since both A and F show ballistic ejection, the apparent opening angle should be the same as the position-angle difference between A and F. Although the apparent opening angle of $\psi_{\rm ob}=26.^\circ 8$ seems to be large, we state that the small viewing angle of the jet magnifies the actual opening angle (ψ) ,

$$\tan \psi_{\rm ob} = \frac{\tan \psi}{\sin \theta}.\tag{8}$$

Taking $\theta \leq 10^{\circ}3$, we have a small opening angle of $\psi \leq 5.^{\circ}1$. Even the apparent small differences of the position angles between the proper motion and the current position are also magnified by projection. For component A, a difference of 4.°7 between the motion and the position vectors should intrinsically be < 1.3 based on its viewing angle. In the case of component F, a difference of 6.6 would be < 1.2. These facts simply support that components A and F follow a ballistic expansion. We also notice that a small difference in the viewing angle can cause a difference in the apparent velocity of components A and F. If we assume the same intrinsic velocity, $\beta = 0.9960$, for A and F, the viewing angle should be 1.8 or 14.08 for component A and 5.01 for F. Though the difference of 9.°7 is larger than the estimated opening angle of 5.°1, a larger intrinsic velocity results in a smaller difference in the viewing angle. We estimated the ejection epochs of components A and F as shown in table 3. Since the epochs are significantly separated by 18.8 ± 0.4 yr, we consider that the ejection is sporadic for each component towards different directions.

While components C2, A, and F have expanded for ~ 20 yr, the bending morphology from component A to F has kept its similarity. If the bending were due to the Kelvin-Helmholtz instability, we would see its growth,

Table 5. Apparent proper motion of the components.

Component	Proper motion (mas yr ⁻¹)	Ejection epoch (yr)	P.A. (°)
C1 C12 C2 A F	0.230 ± 0.006 0.235 ± 0.006	1983.1 ± 3.7 1958.4 ± 1.9 1984.8 ± 0.5 1959.3 ± 0.3 1940.5 ± 0.1	284.3 ± 11 352.0 ± 11 330.9 ± 3.1 324.1 ± 1.9 295.4 ± 0.8

such as the curved motion of component A, and an increase in the bending angle. Since the Kelvin-Helmholtz instability occurs at boundaries between slow and fast flows, we could confirm it by any growth of wiggles or deceleration at the boundary. PW98 reported that the direction of the ridge line near component B apparently swings from P.A. $\simeq 283^{\circ}$ in 1982.9, $\simeq 267^{\circ}$ in 1988.4, \simeq 269° in 1990.8, \simeq 263° in 1992.7, and \simeq 258° in 1993.4. We tried to verify changes in the jet direction by drawing arrows in P.A. = 258° and 283° (see figure 3), but we could not recognize any changes in the jet direction from P.A. = 258° . The self-similar evolution of the pattern implies that the bending represents an internal shock which propagates at the speed of the knots. The very straight motion of A also suggests that the bending presents the appearance of an oblique shock in the jet, rather than the Kelvin-Helmholtz instability. PW98 reported that the jet appears to be bifurcated or edgebrightened in region B in the maps in 1988.4, 1990.8, and 1993.4. We find that the bifurcation starts upstream of component A. Component A is located in the northern stream. The southern stream is separated by ~ 2 mas from component A. The apparent curve of A reported by PW98 may be due to contamination of the southern stream with a lower resolution.

The apparent velocity of C1 is probably slower than that of C2, A, and F. The difference in the apparent velocity between the inner (< 2 mas) and outer jets could indicate that the jet is accelerated in this region, or that C1 exhibits a standing shock. The ejection epoch of C1 in table 5 is not reliable because of an irregularity in the observing frequencies. The behavior of C1 should be monitored by successive VSOP observations.

4.3. Connection to the kpc-Scale Jet

The jet has a straight extension from the core to component A at ~ 50 pc in P.A. $\sim 330^{\circ}$. In the low-resolution images (Wilkinson et al. 1984, 1991; O'Dea et al. 1999), an extended diffuse emission at ~ 4 kpc can be seen in P.A. $\sim 330^{\circ}$. As shown in VLA images by O'Dea et al. (1999), we also see another straight ridge in P.A. $\sim 310^{\circ}$ from 60 pc to 6 kpc scale. The opening angle

of $\sim 27^\circ$ remains even in the kpc-scale jet. This morphology shows that the pc-scale jet straightly connects to the kpc-scale jet, though the brightness is not continuous. For the most simple explanation, the jet keeps its ballistic motion from pc-scale (as shown in components A and F) to kpc-scale, while the position angle of each component is different within the opening angle of $\sim 27^\circ$. Again, we emphasize that the apparent opening angle is magnified due to projection.

5. Conclusions

The first-epoch VSOP observation at 5 GHz towards the superluminal quasar 3C 380 reveals the precise structure and kinematics in the relativistic jet. The core component C is resolved for the first time to appear to have a brightness temperature of $T_b = (4.1 \pm 0.2) \times 10^{11} \text{ K}$, which is attainable without the Doppler boosting effect. On the other hand, components C2, A, and F at projected distances of 19, 55, and 133 pc from the core, respectively, show a superluminal motion. Components A and F have a very straight apparent motion with a constant speed. Considering the projection by small viewing angles of components A and F, each motion vector is parallel to each position vector within 1°3. This fact exhibits that both A and F are moving ballistically away from the core. We cannot confirm any acceleration or changes of P.A. reported by PW98, though we have better position accuracy by a factor of 3. Although the apparent speed seems to increase as the distance increases, it can be explained by a small change in viewing angle without intrinsic acceleration. The slow apparent speed of component C1 should be confirmed by the next-epoch observation. The bending structure from components A to F keeps its similarity with a constant bending angle, while C2, A, and F have expanded during these ~ 20 years. This result supports that the bending can be ascribed to oblique shock in the relativistic flow, rather than the Kelvin-Helmholtz instability.

We gratefully acknowledge the VSOP Project, which is led by the Institute of Space and Astronautical Science (ISAS) in cooperation with many organizations and radio telescopes around the world.

References

Blandford R.D., McKee C.F., Rees M.J. 1977, Nature 267,

Fanaroff B.L., Riley J.M. 1974, MNRAS 167, L31

Fanti R., Fanti C., Schilizzi R.T., Nan R., Parma P., van Breugel W.J.M., Venturi T. 1990, A&A 231, 333

Hirabayashi H., Hirosawa H., Kobayashi H., Murata Y., Edwards P.G., Fomalont E.B., Fujisawa K., Ichikawa T. et al. 1998, Science 281, 1825

Hirosawa H., Hirabayashi H., Kobayashi H., Murata M., Kii T., Edwards P.G., Natori M., Takano T. et al. 1998, in Proc. 49th International Astronautical Congress, IAF-98-Q.1.01

Kameno S., Inoue M., Matsumoto K., Miyaji T., Mikoshiba H., Takaba H., Iwata T., Takahashi Y. et al. 1995, PASJ 47, 711

Marscher A.P. 1987, in Superluminal Radio Sources, ed J.A. Zensus, T.J. Pearson (Cambridge University Press, Cambridge) p280

O'Dea C.P., de Vries W., Biretta J.A., Baum S.A. 1999, AJ 117, 1143

Pearson T.J., Zensus J.A. 1987, in Superluminal Radio Sources, ed J.A. Zensus, T.J. Pearson (Cambridge University Press, Cambridge) p1

Polatidis A.G., Wilkinson P.N. 1998, MNRAS 294, 327 Readhead A.C.S. 1994, ApJ 426, 51

Scott M.A., Readhead A.C.S. 1977, MNRAS 180, 539

Shepherd M.C. 1997, in Astronomical Data Analysis Software and Systems VI, ed G. Hunt, H.E. Payne, ASP Conf. Ser. 125, p77

Taylor G.B. 1998, ApJ 506, 637

Wilkinson P.N., Akujor C.E., Cornwell T.J., Saikia D.J. 1991, MNRAS 248, 86

Wilkinson P.N., Booth R.S., Cornwell T.J., Clark R.R. 1984, Nature 308, 619